Full length article

Copper-containing mesoporous bioactive glass nanoparticles as multifunctional agent for bone regeneration

Alessandra Bari [a,1], Nora Bloise [b,c,1], Sonia Fiorilli [a], Giorgia Novajra [a], Maria Vallet-Regí [d], Giovanna Bruni [e], Almudena Torres-Pardo [f], José M. González-Calbet [f], Livia Visai [b,c], Chiara Vitale-Brovarone [a,*]

[a] Department of Applied Science and Technology, Politecnico di Torino, Corso Duca degli Abruzzi 24, 10129 Torino, Italy
[b] Molecular Medicine Department (DMM), Center for Health Technologies (CHT), UdR INSTM, University of Pavia, Viale Taramelli 3/B, 27100 Pavia, Italy
[c] Department of Occupational Medicine, Toxicology and Environmental Risks, Istituti Clinici Scientifici Maugeri S.p.A, IRCCS, Via S. Boezio 28, 27100 Pavia, Italy
[d] Departamento de Química Inorgánica y Bioinorgánica, Universidad Complutense de Madrid, CIBER de Bioingeniería, Biomateriales y Nanomedicina (CIBER-BBN), Plaza Ramón y Cajal s/n, 28040 Madrid, Spain
[e] Department of Chemistry, Section of Physical Chemistry, University of Pavia, Italy
[f] Departamento de Química Inorgánica, Facultad de Químicas, Universidad Complutense de Madrid, 28040 Madrid, Spain

ARTICLE INFO

ABSTRACT

The application of mesoporous bioactive glasses (MBGs) containing controllable amount of different ions, with the aim to impart antibacterial activity, as well as stimulation of osteogenesis and angiogenesis, is attracting an increasing interest.

In this contribution, in order to endow nano-sized MBG with additional biological functions, the framework of a binary SiO_2-CaO mesoporous glass was modified with different concentrations of copper ions (2 and 5% mol.), through a *one-pot* ultrasound-assisted sol-gel procedure. The Cu-containing MBG (2% mol.) showed high exposed surface area (550 $m^2\,g^{-1}$), uniform mesoporous channels (2.6 nm), remarkable *in vitro* bioactive behaviour and sustained release of Cu^{2+} ions.

Cu-MBG nanoparticles and their ionic dissolution extracts exhibited antibacterial effect against three different bacteria strains, *E. coli*, *S. aureus*, *S. epidermidis*, and the ability to inhibit and disperse the biofilm produced by *S. epidermidis*.

The obtained results suggest that the developed material, which combines in single multifunctional agent excellent bioactivity and antimicrobial ability, offers promising opportunities for the prevention of infectious diseases and the effective treatment of bone defects.

Statement of Significance

In order to endow mesoporous bioactive glass, characterized by excellent bioactive properties, with additional biological functions, Cu-doped mesoporous SiO_2-CaO glass (Cu-MBG) in the form of nanoparticles was prepared by an ultra-sound assisted *one pot* synthesis.
Statement of Significance: The analysis of the bacterial viability, using different bacterial strains, and the morphological observation of the biofilm produced by the *Staphylococcus epidermidis*, revealed the antimicrobial effectiveness of the Cu-MBG and the relative ionic extracts against both the bacterial growth and the biofilm formation/dispersion, providing a true alternative to traditional antibiotic systemic therapies.
Statement of Significance: The proposed multifunctional agent represents a promising and versatile platform for bone and soft tissues regeneration.

1. Introduction

Bone tissue shows an intrinsic potential of self-healing in response to injury [1]. However, the effective treatment of bone defects, especially the larger one resulting from impaired bone regeneration, compromised regenerative process such as

osteoporosis or due to trauma, infection or tumour resection, still represents a challenging clinical issue [2]. To this aim, in the last decades, a wide class of bioactive materials have been proposed as bone-tissue regeneration systems [3,4].

Recently, one of the most appealing approach to design novel biomaterials for bone repair is to combine in a single multifunctional component several abilities, including osteoconductivity (for guidance of new bone growth) and the capacity to stimulate both osteogenesis (for promoting new bone formation) and angiogenesis (for inducing vascularization) [5–7]. Furthermore, bone healing is also substantially hindered when infection occurs, mainly after an open fracture. Conventional treatments include systemic antibiotic administration, surgical debridement or wound drainage [8]. These actions, however, are often ineffective and may result in quite serious complications leading to extra surgeries, with a consequent high burden in terms of pain and social costs. Consequently, the development of bioactive materials enabled with antibacterial properties would represent a valuable solution in preventing post-surgical infections.

In the field of advanced bioceramics, mesoporous bioactive glasses (MBGs), which combine the textural parameters of ordered mesoporous matrices with the properties of conventional bioactive sol-gel glasses, have received increasing attention as bone-tissue regeneration systems [8–14]. The unique textural properties of these templated-glasses, synthesized mostly in the systems SiO_2-CaO or SiO_2-CaO-P_2O_5, lead to significantly enhanced bioactivity compared with conventional bioactive glasses, making them ideal components for bone regeneration. More recently, the application field of MBGs has moved a big step forward by including controllable amount of different ions in their composition. In particular, the final aim is to impart other biological functions, including anti-bacterial activity, as well as stimulation of osteogenesis and angiogenesis, by means of the incorporation of metallic elements with therapeutical effect [15,16]. Furthermore, the large exposed surface area and the accessible pore volume shown by MBGs provide excellent drug delivery ability, which synergistically combined with the release of therapeutic ions, can be exploited for the development of multifunctional biomaterials. In the past five year, different therapeutic ions, including Ag^+, Sr^{2+}, Cu^{2+} and Co^{2+} have been incorporated into MBG-based scaffolds and their release had been related to the enhancement of several biological functions [17–21]. In particular, the release of Sr^{2+} ions from Sr-containing MBG scaffolds was found to significantly stimulate new bone formation in osteoporotic bone defects in vivo [22] and MBG scaffolds incorporating Co^{2+} and Cu^{2+} ions have been reported to promote angiogenesis in vitro and in vivo [23].

Some recent studies have focussed on the development of MBG particles characterized by size ranging from ten to hundreds of nanometres and by excellent surface bioreactivity [24]. This class of nanostructured materials is extremely attractive in relation to regenerative medicine, as it allows to widen the use of MBGs, including the design of nanocomposite with biopolymers, the dispersion as active phase in injectable gels or the production of functional coatings on different materials (porous ceramics, metals) to combine improved mechanical properties and high bioactivity [25–28]. El-Fiqi et al. [29] have recently attained, through an ultrasound-assisted sol-gel process, the preparation of MBG nanoparticles with binary SiO_2-CaO composition, and had shown their capacity to act as delivery nanovehicles of therapeutic molecules, along with excellent apatite forming ability and good cell viability.

In this work, with the aim to endow nano-sized MBGs with additional biological functions, the framework of a binary SiO_2-CaO system was modified with different amount of copper ions, due the recognized therapeutic properties of this element. Indeed, the sustained release of Cu^{2+} ions, as hypoxia-mimicking ion, is known to enhance bone density by inhibiting active bone resorption [30,31]. Furthermore, very recently, a systematic evaluation of copper-doped mesoporous silica nanospheres, through in vitro biological assessment under immune environment, have finely evidenced that these nanomaterials can induce osteogenic/angiogenic factors and suppress osteoclastogenic factors by immune cells, evidencing their potential as immunomodulatory agent for tissue regeneration/therapy applications [32]. Copper is also recognized to be an antimicrobial agent [17], a crucial aspect for an effective bone repair process.

In this contribution, the insertion of Cu ions within the framework of a mesoporous SiO_2-CaO bioglass was carried out through a one-pot ultrasound-assisted sol-gel procedure. The effect of copper insertion on the textural features and the in vitro bioactive response of the resulting systems were assessed, along with the Cu^{2+} release profiles. The antibacterial properties of the synthesized copper containing MBG and their ionic extracts were tested using different bacterial strains. Furthermore, the ability in inhibiting and dispersing the biofilm produced by the Staphylococcus epidermidis was investigated.

2. Materials and methods

2.1. Preparation of Cu-containing MBGs

Copper-loaded MBGs were synthesized through an ultra-sound assisted base catalysed sol-gel method, by incorporating Cu into the MBG framework to replace part of calcium (Ca). MBG with 2% molar percentage of Cu (molar ratio Cu/Ca/Si = 2/13/85, named: Cu_MBG 2%) and 5% molar percentage of Cu (molar ratio Cu/Ca/Si = 5/10/85, named: Cu_MBG 5%) were prepared by the same method. Briefly, 5 g of cetyltrimethylammonium bromide (CTAB, ≥98%, Sigma) was completely dissolved by stirring in 120 mL of absolute methanol, whose pH was adjusted to 12.5 by adding about 30 mL NH$_4$OH. Into this solution, proper amounts of calcium nitrate tetrahydrate (Ca(NO$_3$)$_2$·4H$_2$O, 99%) and copper chloride (CuCl$_2$, 99%) were dissolved. In a separate batch, 0.895 g tetraethyl orthosilicate (TEOS, 99%) were dissolved in 30 mL absolute methanol and was then added to the first solution with the simultaneous application of ultra-sound using a SONOPULS Ultrasonic Homogenizers HD 3200. The output power was 150 W in a 10 s on/10 s off cycle for 20 min. This solution was stirred at room temperature for 24 h. Then the precipitate was separated by centrifugation at 5000 rpm for 5 min, washed one time with distilled water and two times with absolute ethanol. The final precipitate was dried at 70 °C for 12 h and calcined at 600 °C in air for 5 h at a heating rate of 1 °C min^{-1} using a Carbolite 1300 CWF 15/5. A sample without Cu (molar ratio Si/Ca = 85/15, named MBG) was also prepared by the same method and used as reference system.

2.2. Materials characterization

The morphology of the synthesized nanoparticles was analysed by Field-Emission Scanning Electron Microscopy (FE-SEM) microscopy using a Philips 525M instrument. Compositional analysis of the powders was performed by energy dispersive spectroscopy (EDS; Philips Edax 9100).

The samples were characterized by X-ray diffraction (XRD) through a Philips X'pert diffractometer (Cu K$_\alpha$ radiation) and nitrogen adsorption measurements at 77 K performed using a Quantachrome Autosorb 1. Samples were outgassed at 423 K for 5 h before analysis. BET specific surface areas have been calculated in the relative pressure range 0.04–0.1 and the pore size has been evaluated through the DFT (Density Functional Theory) method, using the NLDFT equilibrium model for cylindrical pore.

High Resolution Transmission Electron Microscopy (HRTEM) imaging and local EDS spectroscopy was performed on a JEOL JEM300FEG electron microscope equipped with an ISIS 300 X-ray microanalysis system (Oxford Instruments). Cu_MBG 2% and Cu_MBG 5% samples were ultrasonically dispersed in n-butanol and transferred to carbon coated nickel grids to analyze the copper distribution in the nanospheres.

A PHI 5000 Versaprobe II Scanning X-ray Photoelectron Spectrometer (XPS), equipped with a monochromatic Al K-alpha X-ray source (1486.6 eV energy, 15 kV voltage and 1 mA anode current), was used to investigate the surface chemical composition. A spot size of 100 μm was used in order to collect the photoelectron signal for both the high resolution (HR) and the survey spectra. Different pass energy values were exploited: 187.85 eV for survey spectra and 23.5 eV for HR peaks. The core level spectra were deconvoluted with a nonlinear iterative least squares Gaussian fitting procedure.

2.3. Evaluation of Cu ion release

In order to evaluate Cu ion release, 30 mg of copper-containing samples were placed in a plastic container with 30 mL of SBF (final concentration of 1 mg/mL of SBF) prepared according to Kokubo recipe [33]. The samples were kept immersed for different times up to 7 days at 37 °C in an orbital shaker IKA KS 4000 with an agitation rate of 150 rpm. At each time point, the suspension was centrifuged and 1 mL of the supernatant solution was collected and analysed by inductively coupled plasma atomic emission spectrometry technique (ICP-AES) through the ICPMS Thermoscientific ICAPQ spectrometer.

2.4. Bioactivity assessment

In vitro bioactivity was assessed by using the methodology described in ref [34], where a unified method for the evaluation of HA-forming ability of bioactive glasses in powder form is proposed. In particular, 30 mg of powders MBG and Cu_MBG 2% were soaked in 30 mL of SBF for 3 h, 1, 3, 7 and 14 days. The bottles were placed inside an orbital shaker IKA KS 4000 at a fixed temperature of 37 °C. At each selected time point, the powders were removed by centrifugation at 5000 rpm for 5 min, rinsed with bi-distilled water and dried in oven at 70 °C for 12 h. The pH of SBF was measured at each time point. The powders were analysed by FESEM and by XRD to detect the HA phase formation.

2.5. Antibacterial property of nanoparticles

2.5.1. Bacterial strains and culture conditions

The microorganisms used in this study were Escherichia coli RB (E. coli RB), Staphylococcus aureus 8325-4 (S. aureus 8325-4) and Staphylococcus epidermidis (S. epidermis RP62A), being the later a strong biofilm-producing strain [35,36]. E. coli RB was provided by the "Zooprofilattico Institute of Pavia" (Italy) whereas S. aureus 8325-4 and S. epidermidis RP62-A were kindly supplied by Timothy J. Foster (Department of Microbiology, Dublin, Ireland). All bacteria strains were routinely grown in their culture medium overnight under aerobic conditions at 37 °C using a shaker incubator (New Brunswick Scientific Co., Edison, NJ, USA): E. coli RB in Luria Bertani Broth (LB) (Difco, Detroit, MI, USA), S. aureus 8325-4 in Brian Heart Infusion (BHI) (Difco) and S. epidermidis RP62A in tryptic soy broth (TSB, Difco). These cultures were statically incubated at 37 °C under aerobic conditions and reduced to a final density of 1×10^{10} cells/mL as determined by comparing the optical density (OD_{600}) of the sample with a standard curve relating OD_{600} to cell number.

Two different experimental conditions were used to evaluate the antibacterial activity of un-doped and doped nanoparticles. For the first experimental condition, MBG or Cu_MBG 2% suspensions in sterile phosphate-buffered saline, (PBS: 137 mM NaCl, 2.7 mM KCl, 4.3 mM Na_2HPO_4, pH 7.4) with a final concentration of 2 mg/mL were prepared, sonicated (ultrasonic bath, FALC Instruments, Italy) for 5 min at room temperature, and properly diluted to obtain concentrations of 31, 63, 125, 250, 500, 1000 and 2000 μg/mL. The obtained suspensions were further sonicated for 5 min at room temperature prior to the direct incubation with bacterial cells.

The second experimental condition was analogously performed, but in order to evaluate the antibacterial proprieties ascribable to the released Cu^{2+} ions from Cu_MBG 2%, un-doped and doped MBGs were dispersed in sterile PBS (2 mg/mL) and kept soaked for 3 h and 24 h, then centrifuged and the supernatants collected for antibacterial activity tests. Bacterial strains were incubated without (control) or with increasing serial dilutions of the extracts collected after 3 h and 24 h from the MBG and Cu_MBG 2% suspensions, respectively. The control samples of both the experimental conditions were performed by addition of the same volume of PBS. Each experiment condition was repeated three times.

2.5.2. Evaluation of antibacterial effect on bacterial planktonic growth

For both experimental conditions, a predefined number ($10^{\wedge}4$/mL) of Gram negative (E. coli RB) and Gram positive (S. aureus 8325-4 and S. epidermidis RP62A) cells were incubated in their culture broth at 37 °C in 96-well microtiter plates. For the first experimental condition, bacterial cells were untreated (control) or treated with nanoparticle suspensions at increasing concentrations, ranging from 31 up to 2000 μg/mL, for 1 and 3 days, respectively. For the second experimental condition, bacterial cells were untreated (control) or treated with increasing serial dilutions of extracts previously collected at 3 and 24 h from of MBG or Cu_MBG 2% suspensions (2 mg/mL) and incubated for 1 day.

For both experimental conditions, at fixed incubation times, the quantitative 3-[4,5-dimethylthiazol-2-yl]-2,5 diphenyl tetrazolium bromide (MTT Sigma Aldrich, St Louis, MO, USA) assay was performed to assess the dehydrogenase activity, as an indicator of the metabolic state of cells, as previously described [37]. The bacterial viability was expressed as percentage related to the control set equal to 100%.

2.5.3. Evaluation of antibacterial effect on S. epidermidis biofilms

For biofilm experiments, overnight culture of S. epidermidis RP62A was diluted in its broth culture medium with the addition of 0.25% glucose [38]. Aliquots (100 μL) of the diluted bacterial suspensions were inoculated into 96-well flat-bottom sterile polystyrene microplates (Costar, Corning, NY, USA) as follows: i. without (control) or with a suspension of 2 mg/mL of MBG or Cu_MBG 2% nanoparticles in PBS; ii. without (control) or with extracts collected after 24 h of incubation with MBG or Cu_MBG 2% suspension (2 mg/mL) in PBS. In both cases (i and ii) the experiments were performed in two different types of settings: a. nanoparticles suspensions or nanoparticles extracts were contemporarily incubated with biofilm growing cultures in order to evaluate their effects during biofilm formation; b. nanoparticles suspensions or nanoparticles extracts were added after the biofilm formation, to assess their effects on the formed biofilms. After fixed incubation times, biofilms were washed twice with PBS to remove planktonic cells and loosely adhering bacteria [39]. Viability quantification of microbial cells inhabiting the biofilms was performed by MTT test as described above.

2.5.4. Scanning Electron Microscopy (SEM) of S. epidermidis biofilms

For morphological evaluation, biofilm untreated (control) or treated with nanoparticles suspensions or their extracts for both the experimental settings (as described above) were grown in plastic cell culture coverslip disks (Thermanox Plastic, Nalge Nunc International, Rochester, New York) seeded on the bottom of a 24-well culture plates and incubated for 24 h at 37 °C. Briefly, the disks were washed several times and then fixed for SEM with 2.5% glutaraldehyde in 0.1 M cacodylate buffer, pH 7.2 for 1 h at 4 °C. After additional washes, they were incubated with increasing concentrations of ethanol (25%, 50%, 75% and 96%) for 10 min each, dried to the critical point using an Emitech K-850 apparatus (Emitech, Ashford, Kent, UK) and placed on a mounting base [38]. Finally, the disks were coated with gold layer and examined through SEM analysis (Zeiss EVO-MA10 scanning electron microscope, Carl Zeiss, Oberkochen, Germany).

2.5.5. Statistical analysis

All statistical calculation was carried out using GraphPad Prism 5.0 (GraphPad Inc., San Diego, CA). Statistical analysis was performed using Student's unpaired t-test and through one-way variance analysis (ANOVA), followed by Bonferroni post hoc, for multiple comparisons (significance level of $p \leq 0.05$).

3. Results

3.1. The morphological and structural characterization of Cu_MBGs

The morphology of mesoporous glass nanoparticles doped with defined concentrations of copper ions, was observed by high resolution FE-SEM. The images of Cu_MBG 2% (Fig. 1A) revealed particles with a uniform spheroidal morphology, with size ranging between 170 and 200 nm. Energy-dispersive spectrometry analysis (EDS) confirmed the incorporation of Cu inside the framework: the detected Cu/Si molar ratio, as average of three measurements, resulted in fair agreement with the nominal ratio (Fig. 1B).

TEM observations showed that the nanoparticles contain mesopores throughout their inner structure, in the form of a worm-like system (Fig. 1C). Quantitative analysis using EDS mapping, coupled to TEM, was used to explore the element distribution in the sample and showed that Cu ions, like the other elements, were evenly distributed within the whole of the particle (Fig. 1D).

FE-SEM observation of Cu_MBG 5% sample (Fig. 1E) showed spheroidal particles whose size ranges between 180 and 230 nm, on average slightly larger than what was observed for Cu_MBG 2%. EDS analysis reported in the inset of Fig. 1E showed the incorporation of copper with a molar concentration very close to the nominal ratio. TEM images of Cu_MBG 5%, (Fig. 1F) allowed discerning a core-shell morphology for this sample, with a shell characterized by a regular mesoporous structure and an internal core characterized by larger and irregular cavities. In this case, EDS mapping analysis evidenced different Si, Ca and Cu atomic percentages in the core and shell regions of the particles, showing, a higher concentration of Ca and Cu ions in the core (Ca/Si = 0.13 and Cu/Si = 0.15) compared to the outer shell (Ca/Si = 0.05 and Cu/Si = 0.06).

The mesoporous structure of Cu-modified MBGs systems was confirmed by the N_2 adsorption-desorption isotherms (Fig. 2), which revealed that the isotherm curves of MBG, Cu_MBG 2% and Cu_MBG 5% had type-IV isotherm with a well-defined step at relative pressure (P/P_0) below 0.3, indicative of the filling of uniform mesopores. The capillary condensation observed at higher relative pressures for Cu_MBG 5% (green curve) is ascribable to intra-particles voids or to the disordered porosity located in the particle core, discernible from TEM images.

The values of BET specific surface area, mesopores volume and pore diameter for the investigated samples are reported in Table 1: a decrease of surface area and pore volume was found with increasing the amount of copper ion. The mesopore diameter was approximately 2.6 nm in the Cu-containing samples, which is that typical of CTAB-templated systems.

In the high-angle XRD patterns (Supplementary information, SI.1), the broad peak at 23° corresponded to amorphous silica, and no diffraction peaks of copper oxide (CuO_x) were observed in these samples, indicating that the incorporated copper does not form oxide crystals.

In order to investigate the nature of the copper species incorporated inside the glass framework, XPS spectra were recorded on Cu_MBG 2% and Cu_MBG 5%. Fig. 3 shows the deconvoluted XPS spectra of Cu_MBG 2% and Cu_MBG 5% in the $Cu_{2p3/2}$ region.

The components at 935.7 eV and 933.3 eV obtained through the deconvolution and their integrated peaks areas are reported in Table 2: an evident difference in the relative amount of the two components was found.

3.2. Copper ion release from nanoparticles in SBF

The ionic concentrations (µg/mL) of Cu^{2+} species in SBF medium after contact for 7 days with Cu-containing powders are reported in Fig. 4.

In the case of Cu_MBG 2%, a sustained release of Cu^{2+} is observed over the 7 days of soaking and the percentage released resulted approximately 90%. Furthermore, the EDS analysis of the sample after the release tests did not reveal the presence of residual copper, suggesting a quantitative release of the functional ion. At variance, the release test carried out with Cu_MBG 5% evidenced a very low percentage of released Cu^{2+} (around 10%), suggesting that copper ions are mostly inaccessible.

3.3. Bioactive behaviour of Cu_MGB 2%

Based on the obtained release kinetics for Cu^{2+} species, the investigation about the bioactive properties was uniquely performed on Cu_MBG 2% and on MBG for comparison.

Both samples showed a remarkable bioactivity when soaked in SBF. The precipitation of hydroxyapatite (HA) was assessed after only 3 h of immersion and a conspicuous amount of it could be easily detected after 24 h of soaking.

Fig. 5 shows FE-SEM images of Cu_MBG 2% nanoparticles after 3 (Fig. 5A) and 7 days (Fig. 5B) and related EDS spectra (Fig. 5D′ and D″) of SBF soaking: globe-shaped agglomerates are easily distinguishable on the nanoparticles surface. The phase nucleated after 3 h of soaking, as assessed by EDS analysis, can be identified as Ca-deficient HA (Ca/P = 1.51). The Ca content in the newly formed phase gradually rises as soaking time increases and after seven days, a molar Ca/P ratio of 1.62 was detected, which is in the range of calcium-deficient biological apatite. The pH of SBF remained in the physiological range during particles soaking (between 7.4 and 7.5).

The WAXRD spectrum of the Cu_MBG 2% sample after 24 h of soaking in SBF is reported in Fig. 5C. Marked peaks at 32° and 26° and other less intense reflections at about 40°, 47° and 49° were assigned to the $(0\,0\,2)$, $(2\,1\,1)$, $(3\,0\,0)$, and $(2\,1\,3)$ reflections of HA (reference code 01-074-0565). The other narrow peaks are ascribable to calcite (reference code 01-083-1762).

3.4. Antibacterial property of MBG nanoparticles and their extracts on bacterial planktonic growth

In the present study, the synthesized nanoparticles (first experimental condition) and their extracts (second experimental
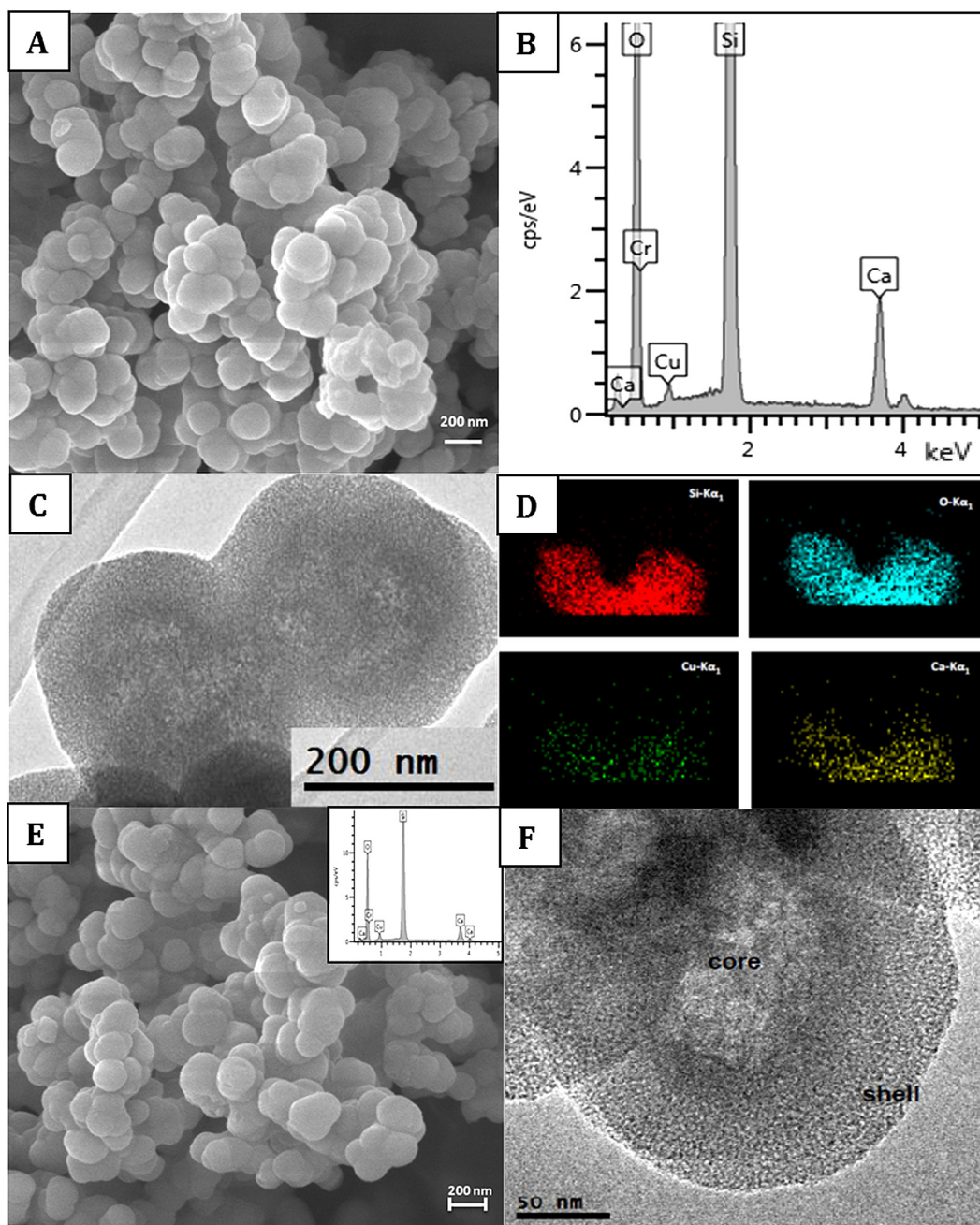
Fig. 1. SEM image of Cu_MBG 2% (A), EDS spectrum (B), TEM image (C) and EDS mapping analysis of Cu_MBG 2% (D), Si (red), O (blue), Cu (green) and Ca (yellow) are uniformly distributed in the nanoparticles; SEM image of Cu_MBG 5% (E), related EDS spectrum (inset), TEM image (F). (For interpretation of the references to colour in this figure legend, the reader is referred to the web version of this article.)

condition) were tested for their antibacterial activity against human pathogenic bacteria, namely, *E. coli RB*, *S. aureus* 8325-4 and *S. epidermidis* RP62A (Figs. 6 and 7). For the first condition (Fig. 6), all the bacteria strains were incubated with different concentrations of both MBG and Cu_MBG 2% particles for 1 and 3 days of culture, respectively. The results in Fig. 6 evidenced a similar trend on all bacteria cultures after the incubation with the Cu_MBG 2% nanoparticles, showing that the bacterial growth suppression was clearly correlated to the presence of copper and its increasing availability for higher concentration. After 1 day of incubation with a concentration above 250 μg/mL, approximately 30–40% of growth inhibition was observed for all types of bacteria, in comparison to the control (cultures without nanoparticles). In particular, the obtained results showed that at longer incubation times

(3 days) with the higher suspension concentration (2 mg/mL), the reduction of viability for both *E. coli RB* and *S. aureus* 8325-4 cultures was 70–75%, and for *S. epidermidis* around 50%.

Compared to MBG cultures both at short and long incubation times, *E. coli RB* and *S. aureus* showed a slightly lower cell viability using 2 mg/mL or 500 μg/mL of Cu_MBG 2%, respectively. At variance, with *S. epidermidis*, the difference in cell viability was dose-dependent, starting from the lower concentrations and becoming more evident at the higher doses (Fig. 6). Interestingly, the results showed that MBG, although not containing copper, exhibited a slight antibacterial effect against the *E. coli RB* and *S. aureus* (around 25%) remaining persistent at all the tested concentrations (not dose-dependent). On the contrary, with *S. epidermidis* cultures, the obtained results highlighted a clear effect related to copper,
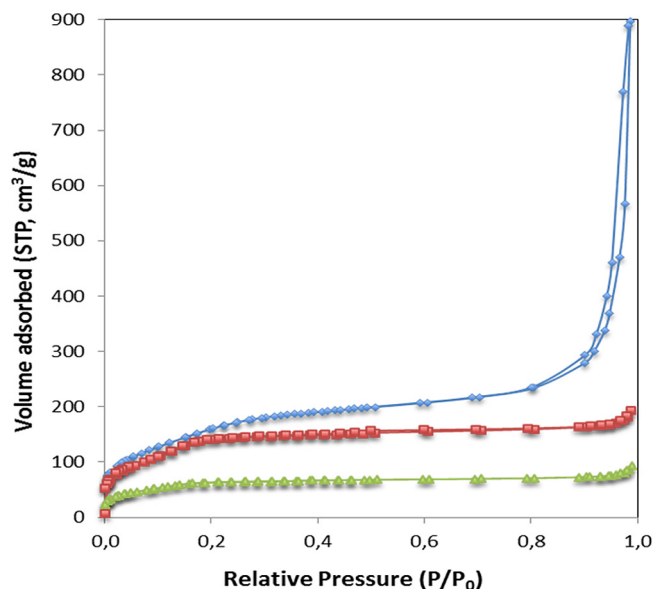
Fig. 2. N_2 adsorption-desorption isotherms of MBG (blue), Cu_MBG 2% (red) and Cu_MBG 5% (green) show type IV curve with H1 hysteresis, indicative of a mesoporous structure. (For interpretation of the references to colour in this figure legend, the reader is referred to the web version of this article.)

Table 1
Structural features of MBG, Cu_MBG 2% and Cu_MBG 5% samples.

Samples	Specific Surface ($m^2\,g^{-1}$)	Pore Volume ($cm^3\,g^{-1}$)	DFT Pore Size (nm)
MBG	621	1.05	2.9
Cu_MBG 2%	550	0.26	2.6
Cu_MBG 5%	224	0.11	2.6

suggesting a different sensitivity of bacteria to the MBG composition and most likely a different antibacterial mechanism of action (Fig. 6).

In order to evaluate the influence of the released copper on the antibacterial effect, the same experiments were performed in parallel with both MBG and Cu_MBG 2% extracts (Fig. 7). Overall, it was clear that there was a positive correlation between the extracts concentrations and bacteria growth inhibition, showing the same trend observed in the experiments based on the direct contact with nanoparticles. Interestingly, in all bacteria cultures, a cell viability reduction was observed in the samples treated with extract of Cu_MBG 2% collected after 24 h (Fig. 7B), if compared with extracts from MBG, hence confirming the role of copper in the observed antibacterial activity. The same experiments carried out with extracts of Cu_MBG 2% and MBG collected after 3 h revealed a rather varying trend in the bacterial viability for all the tested strains, which did not allow a reliable interpretation of the data obtained for such short incubation times (Fig. 7A).

3.5. Antibacterial effect of nanoparticles and their extracts on S. epidermidis biofilm

S. epidermidis RP62A is known to produce considerable quantities of polysaccharide intercellular adhesions, inducing biofilm formation [35,40]. To evaluate the antibacterial activity on staphylococcal biofilms, *S. epidermidis* cultures were incubated with MBG and Cu_MBG 2% suspensions (2 mg/mL) or with related extracts collected after 24 h of incubation, either during the biofilm formation or in the presence of pre-formed biofilms (Figs. 8 and 9). A significant reduction of biofilm growth was determined when the cultures were performed in the presence of Cu_MBG 2% particles if compared to MBG (Fig. 8A, indicated by ∗∗∗) and untreated cultures (data not shown). Moreover, a significant difference in cell viability was obtained when a stable formed biofilm was treated
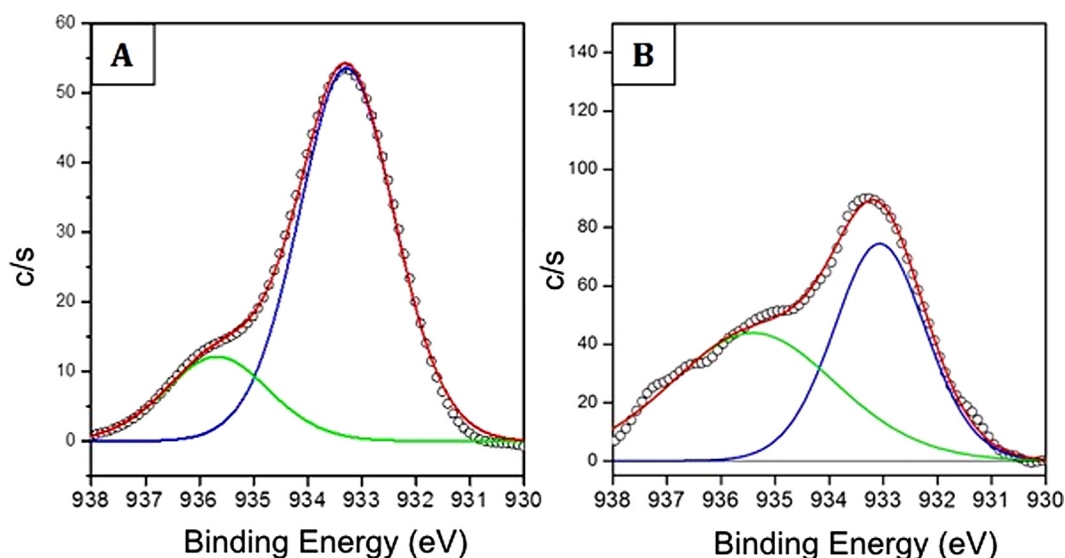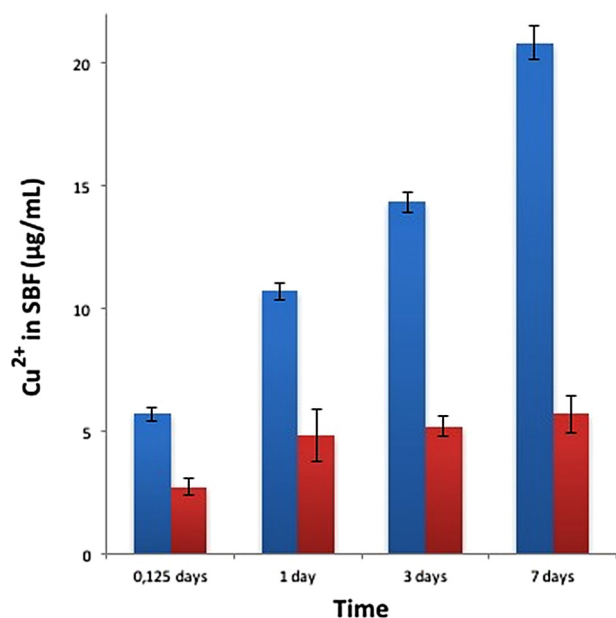

Fig. 3. The XPS deconvoluted spectra in the $Cu_{2p3/2}$ region for Cu_MBG 2% (A) and Cu_MBG 5% (B).

Table 2
Deconvoluted contributions of Cu2p core level and relative percentages.

|	Peak position (eV)	Peak area%	Peak position (eV)	Peak area%
Cu_MBG 2%	933.3	80.3	935.7	19.7
Cu_MBG 5%	933.3	48.5	935.7	51.5

Fig. 4. Cu^{2+} release profiles of Cu_MBG 2% (blue) and Cu_MBG 5% (red) in SBF. (For interpretation of the references to colour in this figure legend, the reader is referred to the web version of this article.)

with MBG or Cu_MBG 2% nanoparticles (Fig. 8C, indicated by ∗∗). Conversely, these effects were less marked in the presence of only copper containing extracts (released by nanoparticles) when incubated during the biofilms formation (Fig. 9A) or on the pre-formed biofilms (Fig. 9C).

Furthermore, in order to visualize the biofilms morphology after these treatments, SEM studies were carried out. As expected, large cellular aggregates were observed in the biofilms produced by *S. epidermidis* RP62A in all samples used as control (Figs. 8B and D; 9B and D). Conversely, the presence of nanoparticles during *S. epidermidis* biofilm formation prevented and reduced the number of adherent bacteria and cluster formation, more distinctly for Cu_MBG 2% nanoparticles (Fig. 8B‴). The addition of Cu_MBG 2% suspension to an already formed staphylococcal biofilm, promoted a visible dispersion of biofilm aggregates (Fig. 8D‴) whereas the contact with MBG suspension produced a less noticeable influence on the biofilm morphology. Similar results were observed for biofilm growing cultures (Fig. 9B‴) or for formed biofilms (Fig. 9D‴) incubated with Cu_MBG 2% extracts, although the bacterial reduction was less evident in comparison to biofilms treated with Cu_MBG 2% suspensions.

4. Discussion

In this study, a novel therapeutic Cu-doped mesoporous SiO_2-CaO glass was successfully obtained by a *one-pot* sol-gel synthesis
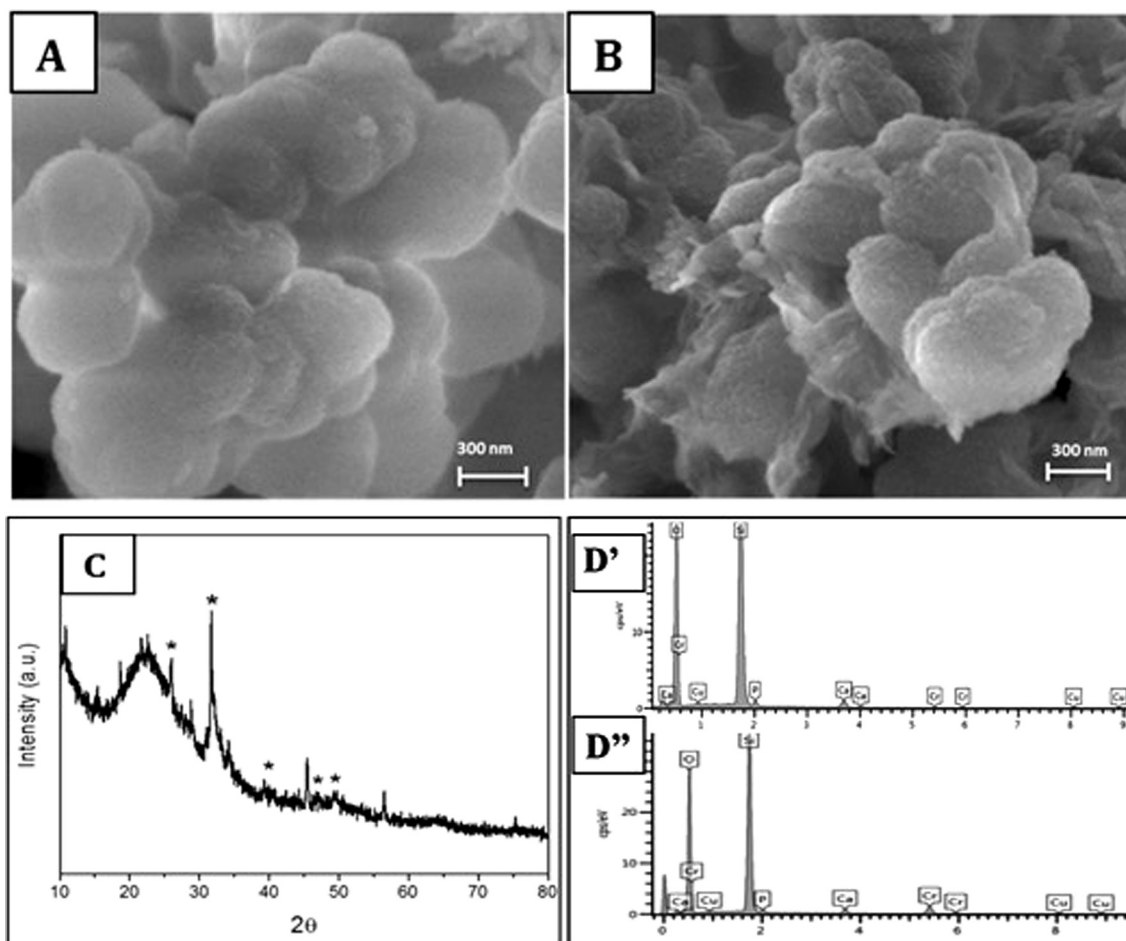
Fig. 5. SEM images of Cu_MBG 2% after 3 days (A) and 7 days (B) of soaking in SBF and XRD pattern of Cu_MBG 2% after soaking in SBF for 7 days (C): the peaks marked with asterisks are due to hydroxyapatite phase; EDX spectra of Cu_MBG 2% after 3 days (D′) and 7 days (D″) of soaking in SBF.
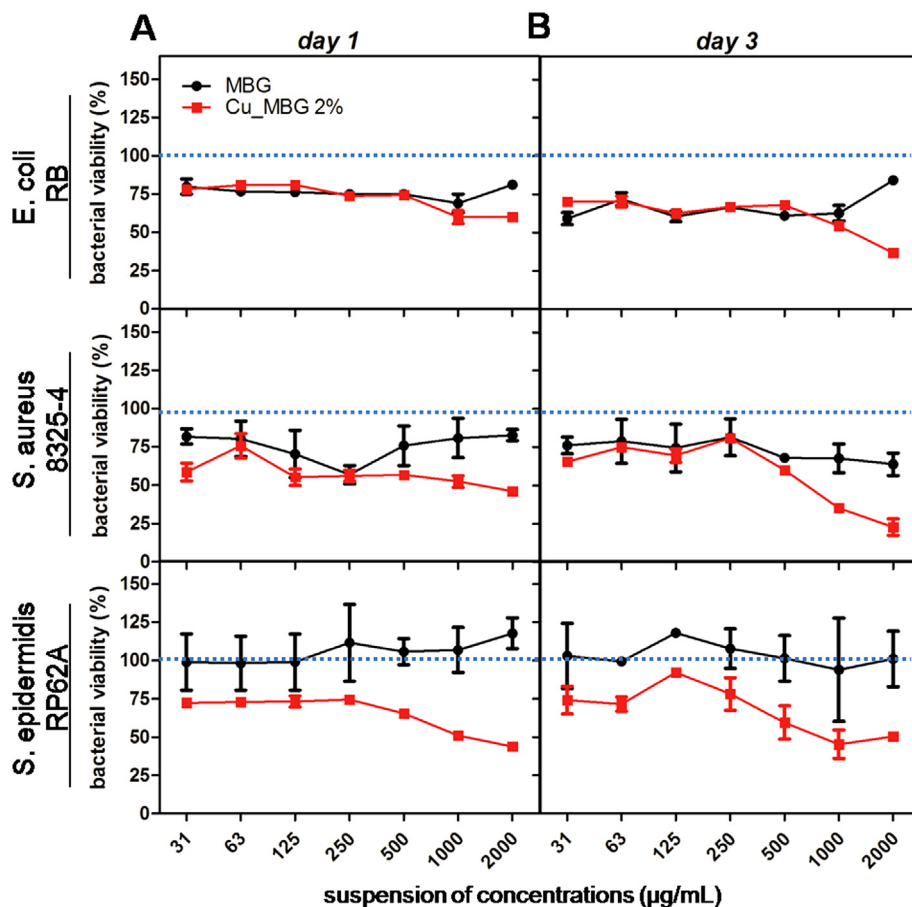
Fig. 6. Dose-dependence viability of different bacterial strains cultured with MBG and Cu_MBG 2% suspensions. Gram-negative (*E. coli* RB) and gram-positive (*S. aureus* 8325-4 and *S. epidermidis* RP62A) bacterial strains were incubated with MBG or Cu_MBG 2% suspensions with concentrations in the range of 31–2000 µg/mL. After 1 and 3 days of incubation, MTT assay was performed in all samples to evaluate cell viability expressed as percentage of viability determined in the absence of nanoparticles (set to 100%).

combined with high-frequency ultrasonication treatment. This method allowed us to obtain Cu-containing mesoporous spheroidal particles with rather homogeneous size, very high exposed surface area and uniform mesoporous channels. Two different amounts of Cu^{2+} ion were incorporated inside the glass framework, leading to systems characterized by evident changes in terms of exposed surface area and release properties of Cu^{2+} ion. Specifically, the increase of copper amount in the synthesis had a negative effect, affecting the formation of the mesostructure and leading to a significant decrease of both exposed surface area and pore volume. These results confirm that the presence of an excess of metal ions species in the reaction plays a negative role on the condensation of the silica precursors and the assembly of the mesophase structure [32,41], leading to a significant decrease of the exposed surface area in the obtained material.

TEM observations further confirmed that higher amount of doping cation had an evident impact on the structural properties of the produced MBGs. Specifically, Cu_MBG 5%, at variance with Cu_MBG 2%, shows particles characterized by a marked core-shell morphology and, as highlighted by EDS mapping analysis, by an enrichment of copper in the core compared to the outer shell.

The nature of incorporated copper species was analysed by XPS analysis, which evidenced a sizeable difference in the relative concentration of detected Cu^{2+} species. A first component at lower binding energy (933.3 eV) is consistent with values ascribed in the literature to Cu^{2+} cations in extra-framework sites [42]. At variance, the component at higher binding energy, at *ca* 935.7 eV, much higher than that for pure CuO (ca 933.8 eV) [43], is attributed

to copper species with a strong electronic interaction with the lattice, in analogy with results obtained for Cu-doped mesoporous silicas [44]. Specifically, for the Cu_MBG 2% (Fig. 3A) sample most of copper species are characterized by binding energy (933.3 eV) typical of extra-framework sites, with a limited contribution of species at higher values, whereas the Cu_MBG 5% sample, as reported in Fig. 3.B, shows a significant higher amount of Cu^{2+} at higher binding energy (935.7 eV). The chemical environment of the incorporated copper species plays an essential role in determining the different release behaviour observed for the samples. The Cu_MBG 2% sample showed a sustained almost complete release of the incorporated Cu^{2+}, which supports the assignment proposed for the component at 933.3 eV to species present as counter-ions of the silica framework, located at the mesopore surface and thus accessible for cation-exchange reactions when soaked in SBF. On the other hand, the unexpected profile observed for Cu_MBG 5%, characterized by a very limited release of Cu^{2+} species, could be interpreted assuming the inaccessibility of mostly of the incorporated metal, as it is likely located in the particle cores or embedded into the silica walls.

The Cu^{2+} release profile obtained for Cu_MBG 2% is in good agreement with that reported for Cu-containing silica nanospheres by Wu and co-workers [32], who investigated the effect of this functional ion as osteoimmunomodulatory agent and as angiogenesis promoter, suggesting similar properties for copper when released from MBG matrices.

The *in vitro* bioactive response of Cu_MBG 2%, in terms of apatite-like forming ability, assessed through soaking in SBF, was
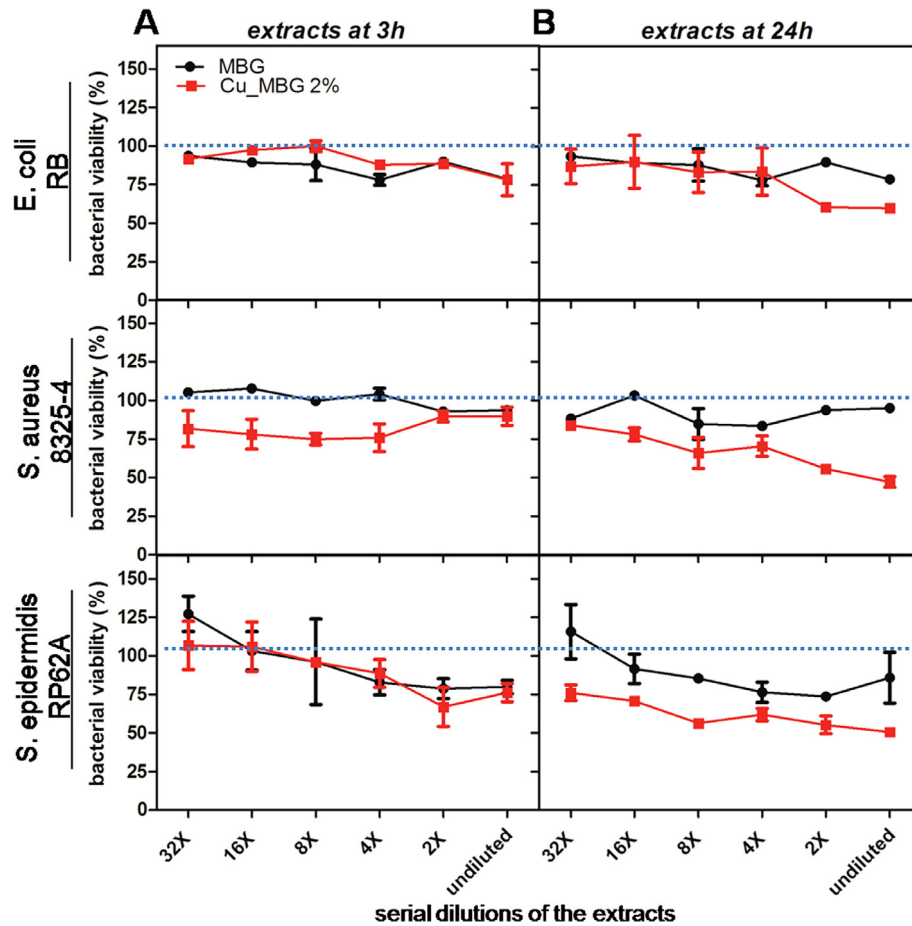
Fig. 7. Dose-dependence viability of different bacterial strains cultured with MBG and Cu_MBG 2% extracts. Gram-negative (*E. coli* RB) and gram-positive (*S. aureus* 8325-4 and *S. epidermidis* RP62A) bacterial strains were incubated without (control) or with increasing serial dilutions of the extracts collected after 3 (A) and 24 h (B) from 2 mg/mL suspension of MBG or Cu_MBG 2% nanoparticles, respectively. After 1 day of incubation, MTT assay was performed in all samples to evaluate the viability expressed as percentage of bacterial viability compared to control (set to 100%).
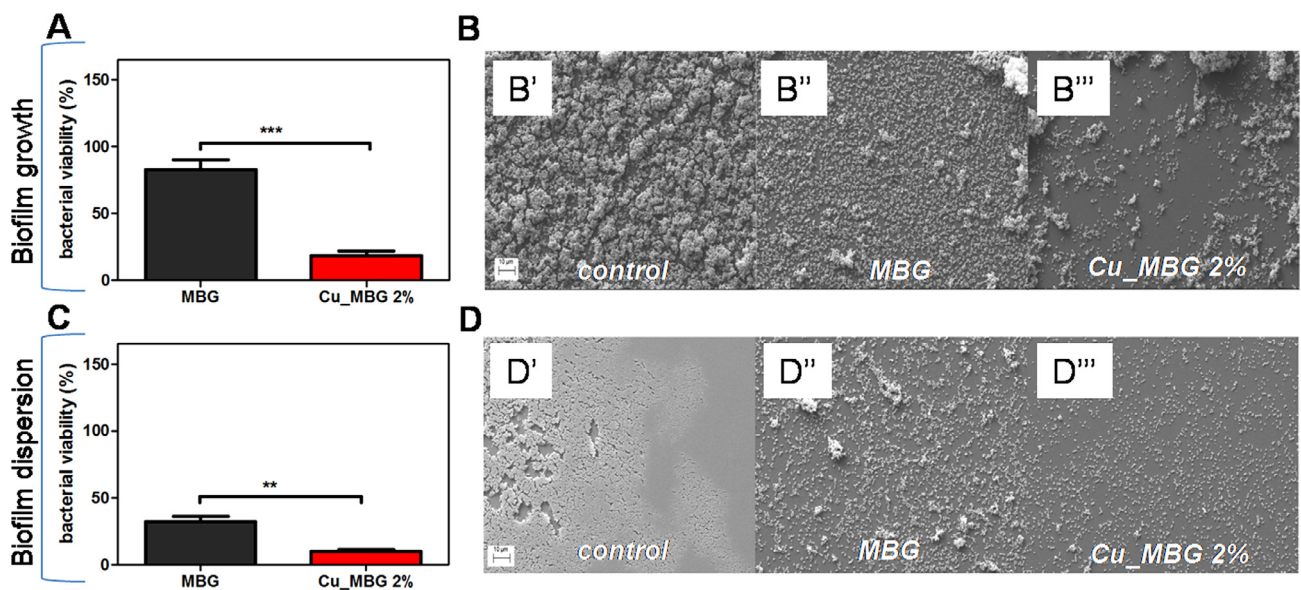
Fig. 8. Bacterial viability and morphology of biofilms treated with MBG and Cu_MBG 2% suspensions (2 mg/mL). Both MBG or Cu_MBG 2% suspensions were added to *S. epidermidis* RP62A biofilm formation cultures (A) or after the formation of a stable staphylococcal biofilm (C). The biofilms cell viability was measured with the MTT assay after 24 h of incubation in both experimental conditions. Results were expressed as percentage of the control (w/o nanoparticles). SEM representative images of the staphylococcal biofilms formed in the absence (control) or in contact with both types of nanoparticles for 24 h are shown (B). SEM images of post formed biofilms, untreated (control) or treated with both MBG or Cu_MBG 2% nanoparticles for 24 h, are also presented (D). Magnification, 2kx.
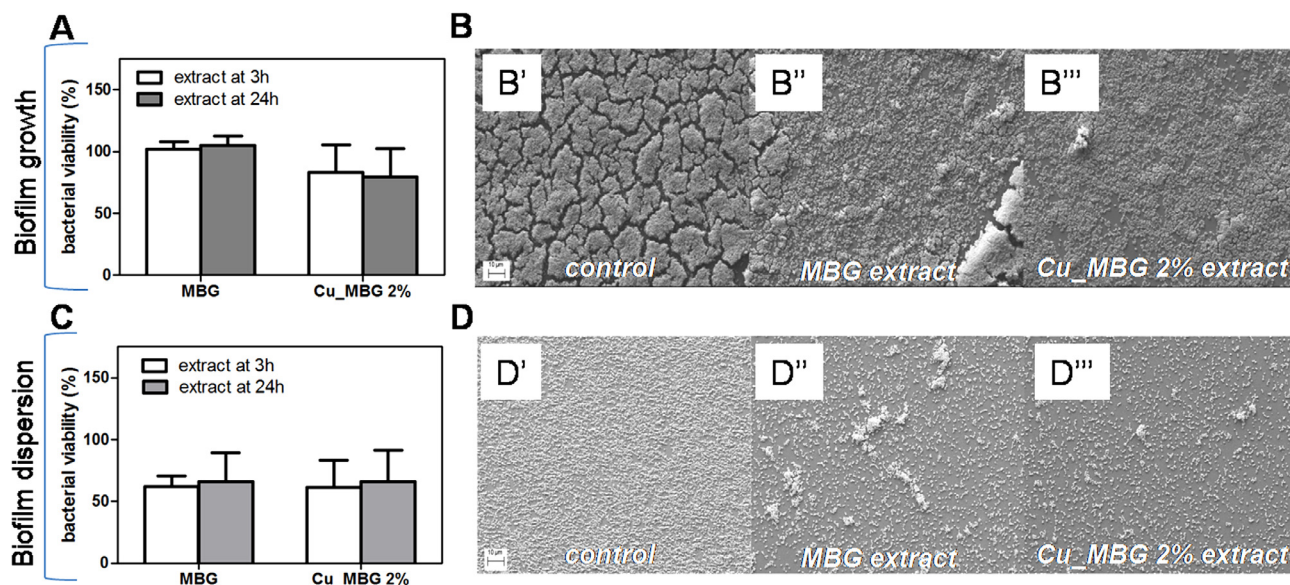
Fig. 9. Bacterial viability and morphology of biofilms treated with extracts of MBG and Cu_MBG 2%. Undiluted supernatants collected at 24 h from 2 mg/mL of both types of nanoparticle suspensions were added to *S. epidermidis* RP62A biofilm growing cultures (A) or after the formation of a stable staphylococcal biofilm (C). The biofilm viability was measured with the MTT assay after 24 h of incubation. Results were expressed as percentage of the control. SEM images of staphylococcal biofilm formed without (control) or with extracts for 24 h are shown (B). SEM images of post formed biofilms, incubated w/o (control) or with extracts for 24 h are also presented (D). Magnification, 2kx.

found to be similar to un-doped MBG systems [10]. Besides the typical peaks due to hydroxyapatite phase, the XRD pattern revealed the components ascribed to calcite precipitate. The latter is often found when bioactive glasses with a high content of calcium (at least 30% mol of CaO) are soaked in SBF. These glasses, when in contact with water-based solutions, release immediately a high amount of Ca^{2+} ions, which, in the case of SBF, react with the carbonate ions present, leading to calcite precipitation within the very first hours of immersion [45–47]. Although the calcium content for Cu_MBG 2% sample is not as high as reported in the literature, the very high exposed surface, due to the presence of the mesopores, is expected to allow a high release of calcium ions in terms of both the total amount and the kinetics. Calcite has been reported to be resorbable [48] and osteoconductive, even without the formation of a Ca-P-rich layer [49]. Therefore, the co-precipitation of apatite and calcite can be considered as an index of the mesoporous glass bioactivity [50].

As stated above, previous studies have documented the excellent antibacterial function of soluble copper compounds against many microorganisms [51,52]. In recent years, the interest in adding metals (e.g. silver, copper, zinc), with proved antimicrobial activity, to innovative nanoparticles and nanocomposites [53], with the final aim to reduce or prevent a device-related infection, and to reduce or inhibit bacterial colonization has grown. In the present study, the antibacterial effect of Cu-doped mesoporous bioglass nanoparticles against two gram-positive bacteria (*S. aureus* and *S. epidermidis)* and one gram-negative (*E. coli)*, was investigated. In agreement with the literature related to Cu-containing nanocomposite systems [54], the results obtained in this work, confirmed that the release of Cu^{2+} ions plays a fundamental role on antimicrobial properties. The antibacterial effect and the mechanism of action of copper on bacteria viability is not fully elucidated yet, however, it seems to be mainly associated to the pleiotropic effects of copper on bacterial cells, through a multiple mechanism of action. The results obtained in this work evidenced that Cu-doped glass nanoparticles showed antimicrobial effect, highly dependent to the dose and bacterial strains. The remarkable difference might be attributed to the different properties of

bacteria surfaces [55]. In gram-positive bacteria, the absence of an outer membrane and the presence of surface negatively charged teichuronic and lipoteichoic acids within a single lipid bilayer surrounded by a thick but porous layer of peptidoglycan (20–80 nm), make them attractive to positively charges [56]. Therefore, the inhibiting process is supposed to be most likely associated to the action of released metal ions, which might be easily moved inside the microbial cells or attached to the charged outer surfaces by electrostatic attraction, resulting in cell apoptosis via protein denaturation and disruption of cell membrane [57]. By contrast, gram-negative bacteria expose a highly organized compact structure, which acts as a permeability barrier and prevents diffusion to the inner plasma membrane for most high molecular weight compounds, making them less attractive to metal nanoparticles treatment. Moreover, the presence of copper tolerance mechanisms in *E. coli* [58], including the activation transmembrane copper export occurring from cytoplasm into the periplasmic space or into the extracellular milieu and the copper sequestration by metallothioneins, can further explain the requirement of a higher Cu_MBG concentrations to inhibit *E. coli* cultures in comparison to the other bacterial strains.

At variance in *E. coli* and *S. aureus* bacteria, the Cu-doped MBG antibacterial effect seems not to be merely due to the release of metal ions in solution, but most likely the small size and the high surface-to-volume ratio of Cu_MBG particles, account for the activation of cell death mechanisms [59,60]. In this regard, further investigations are certainly required in order to fully elucidate the mechanisms involved in the antimicrobial activity of the investigated systems.

Remarkably, this non-specific mode of action of copper-based systems makes them powerful antimicrobial agents with an intrinsic low likelihood of inducing microbial resistance [61].

In recent years, the number of infections associated with antibiotic-resistant bacteria has greatly increased. Many of these infections are caused by microorganisms growing in biofilms, complex bacterial communities surrounded by a self-producing extracellular polymer matrix, able to resist both to antibiotic action and to human immune system [62]. The formation of biofilm is a

peculiar characteristic of *S. aureus* and *S. epidermidis* [63] that quite frequently colonise medical devices, causing persistent body-related infections.

Unlike planktonic populations, bacterial cells embedded in biofilms exhibit intrinsic resistance to antibiotics due to several specific defence mechanisms conferred by the biofilm environment, including the inactivation of anti-microbial agents by exopolysaccharide (EPS), over expression of stress-responsive genes, oxygen gradients within the biofilm matrix and differentiation of a subpopulation of biofilm cells into resistant dormant cells [64,65]. The aforementioned features of biofilms place them amongst the most serious problems currently faced by medicine and thus considerable efforts are devoted to identify novel therapies to prevent or treat biofilms. To this purpose, a potentially promising treatment implies metal or metal oxide nanoparticles, showing antibacterial and anti-biofilm activity [66–68].

In the present work, the obtained data showed that Cu_MBG 2% nanoparticles, inhibited he bacterial growth and were also able to counteract the formation of biofilm produced by *S. epidermidis* and even to favour its dispersion.

The evidence of biofilm inhibition and dispersion was provided both from the assessment of the bacterial viability and from the morphological observations of biofilm through SEM analysis. Cu_MBG 2% nanoparticles dramatically decreased the number of viable cells within the tested biofilms and SEM results shows a significant reduction of surface coverage by *S. epidermidis* biofilms. Considering the widespread occurrence and significant impact of *S. epidermidis* biofilms in a variety of clinical settings, the developed antimicrobial material offer promising opportunities for the prevention of infectious diseases.

Consistent with other studies [17,61,69,70], these findings provide further proof of copper antimicrobial effectiveness against both the bacterial growth and the biofilm formation and dispersion, offering a powerful alternative to traditional systemic therapies based on antibiotics.

Antibiotic resistance is a major challenge in the treatment of infectious diseases, particularly due to the emergence of multidrug-resistant pathogenic strains (MDR). Thus, in perspective, the system proposed in the present study, due to the combination of excellent antibacterial and bioactive properties, represents an effective agent, alone or in synergy with complementary approaches, for the treatment of bacterial diseases associated to orthopaedic implant infections. The synergistic action of Cu-doped MBGs nanoparticles, for instance in combination with various antibiotics, could result in excellent inhibition of bacteria in planktonic stage, reducing the therapeutic dose to treat the bacterial infections and thereby reducing the toxicity risks. Moreover, based on the observed anti-biofilm results, it could be envisaged their application as antibacterial coatings of medical implants, to make these devices more resistant to the bacterial colonization and biofilm formation.

5. Conclusions

In this study, a novel Cu-containing mesoporous bioactive glass (Cu_MBG), in the form of spheroidal nanoparticles, was synthesized via an efficient one-pot synthesis procedure. The incorporation of copper within the SiO_2-CaO framework (up to 2% mol.) led to a material characterized by very high specific surface area, uniform mesopores, homogeneous distribution of copper, excellent bioactive behaviour and the ability to release the copper ions at a sustained rate in a biological buffer solution. The assessment of the antibacterial properties of Cu_MBG nanoparticles and their ionic extracts against *E. coli, S. aureus* and *S. epidermidis* showed a very effective antibacterial ability against all the tested bacteria

strains, with a strain-dependent effect. A fundamental role on the observed antibacterial activity was ascribed to copper ions released by Cu_MBG particles, as highlighted by the reduction of bacterial viability in the presence of their dissolution ionic extracts. Furthermore, Cu_MBG 2% suspension, at proper concentration, is able to reduce and disrupt the biofilm matrix.

Based on the these results, Cu_MBG shows a great potential as multifunctional therapeutic agent for preventing diseases related to infections and for stimulating bone regeneration.

Appendix A. Supplementary data

Supplementary data associated with this article can be found, in the online version, at http://dx.doi.org/10.1016/j.actbio.2017.04.012.

References

[1] P.J. Harwood, D.O. Ferguson, (ii) An update on fracture healing and non-union, Orthop. Trauma 29 (2015) 228–242.
[2] R. Dimitriou, E. Jones, D. McGonagle, P.V. Giannoudis, Bone regeneration: current concepts and future directions, BMC Med. 9 (2011) 66–75.
[3] L.L. Hench, I. Thompson, Twenty-first century challenges for biomaterials, J. R. Soc. Interface 7 (2010) 379–391.
[4] T.G. Kim, H. Shin, D.W. Lim, Biomimetic scaffolds for tissue engineering, Adv. Funct. Mater. 22 (2012) 2446–2468.
[5] I. Denry, L.T. Kuhn, Design and characterization of calcium phosphate ceramic scaffolds for bone tissue engineering, Dent. Mater. 32 (2016) 43–53.
[6] C. Wang, Y. Xue, K. Lin, J. Lu, J. Chang, J. Sun, The enhancement of bone regeneration by a combination of osteoconductivity and osteostimulation using beta-CaSiO3/beta-Ca$_3$(PO$_4$)$_2$ composite bioceramics, Acta Biomater. 8 (2012) 350–360.
[7] Y.C. Hu, J.P. Zhong, Osteostimulation of bioglass, Chin. Med. J. (Engl) 122 (2009) 2386–2395.
[8] L.Z. Zhao, X.X. Yan, X.F. Zhou, L. Zhou, H.N. Wang, H.W. Tang, C. Yu, Mesoporous bioactive glasses for controlled drug release, Microporous Mesoporous Mater. 109 (2008) 210–215.
[9] X. Yan, C. Yu, X. Zhou, J. Tang, D. Zhao, Highly ordered mesoporous bioactive glasses with superior in vitro bone-forming bioactivities, Angew. Chem. Int. (Engl) 43 (2004) 5980–5984.
[10] M. Vallet-Regi, L. Ruiz-Gonzalez, I. Izquierdo-Barba, J.M. Gonzalez-Calbet, Revisiting silica based ordered mesoporous materials: medical applications, J. Mater. Chem. 16 (2006) 26–31.
[11] A. López-Noriega, D. Arcos, I. Izquierdo-Barba, Y. Sakamoto, O. Terasaki, M. Vallet-Regí, Ordered mesoporous bioactive glasses for bone tissue regeneration, Chem. Mater. 18 (2006) 3137–3144.
[12] M. Vallet-Regí, I. Izquierdo-Barba, M. Colilla, Structure and functionalization of mesoporous bioceramics for bone tissue regeneration and local drug delivery, Philos. Trans. R. Soc. A 370 (2012) 1400–1421.
[13] F. Tang, L. Li, D. Chen, Mesoporous silica nanoparticles: synthesis, biocompatibility and drug delivery, Adv. Mater. 24 (2012) 1504–1534.
[14] D. Ling, L. Gao, J. Wang, M. Shokouhimehr, J. Liu, Y. Yu, M.J. Hackett, P. So, B. Zheng, Z. Yao, J. Xia, T. Hyeon, A general strategy for site-directed enzyme immobilization by using NiO nanoparticle decorated mesoporous silica, Chem. Eur. J. 20 (2014) 7916–7921.
[15] C. Wu, J. Chang, Multifunctional mesoporous bioactive glasses for effective delivery of therapeutic ions and drug/growth factors, J. Controlled Rel. 193 (2014) 282–295.
[16] M. Erol-Taygun, K. Zheng, A.R. Boccaccini, Nanoscale bioactive glasses in medical applications, Int. J. Appl. Glass Sci. 4 (2013) 136–148.
[17] C. Wu, Y. Zhou, M. Xu, P. Han, L. Chen, J. Chang, Y. Xiao, Copper-containing mesoporous bioactive glass scaffolds with multifunctional properties of angiogenesis capacity, osteostimulation and antibacterial activity, Biomaterials 34 (2013) 422–433.
[18] H.M. Lin, J. Zhang, F.Y. Qu, J.J. Jiang, P.P. Jiang, In vitro hydroxyapatite-forming ability and antimicrobial properties of mesoporous bioactive glasses doped with Ti/Ag, J. Nanomater. 2013 (2013) 786420–786428.
[19] N. Gargiulo, A.M. Cusano, F. Causa, D. Caputo, P.A. Netti, Silver-containing mesoporous bioactive glass with improved antibacterial properties, J. Mater. Sci. Mater. Med. 24 (2013) 2129–2135.

[20] Y. Zhu, X. Li, J. Yang, S. Wang, H. Gao, N. Hanagata, Composition-structure-property relationship of the CaO-MxOy-SiO2-P2O5 (M = Zr, Mg, Sr) mesoporous bioactive glass (MBG) scaffolds, J. Mater. Chem. 21 (2011) 9208–9218.

[21] C. Wu, Y. Zhou, C. Lin, J. Chang, Y. Xiao, Strontium-containing mesoporous bioactive glass scaffolds with improved osteogenic/cementogenic differentiation of periodontal ligament cells for periodontal tissue engineering, Acta Biomater. 8 (2012) 3805–3815.

[22] Y.F. Zhang, L.F. Wei, J. Chang, R.J. Miron, B. Shi, S.Q. Yi, C.T. Wu, Strontium incorporated mesoporous bioactive glass scaffolds stimulating in vitro proliferation and differentiation of bone marrow stromal cells and in vivo regeneration of osteoporotic bone defects, J. Mater. Chem. B 1 (2013) 5711–5722.

[23] C. Wu, Y. Zhou, W. Fan, P. Han, J. Chang, J. Yuen, M. Zhang, Y. Xiao, Hypoxia-mimicking mesoporous bioactive glass scaffolds with controllable cobalt ion release for bone tissue engineering, Biomaterials 33 (2012) 2076–2085.

[24] C. Wu, J. Chang, W. Fan, Bioactive mesoporous calcium–silicate nanoparticles with excellent mineralization ability, osteostimulation, drug-delivery and antibacterial properties for filling apex roots of teeth, J. Mater. Chem. 22 (2012) 16801–16809.

[25] G.M. Luz, J.F. Mano, Preparation and characterization of bioactive glass nanoparticles prepared by sol-gel for biomedical applications, Nanotechnology 22 (2011) 494014.

[26] S. Labbaf, O. Tsigkoua, K.H. Muller, M.M. Stevens, A.E. Porter, J.R. Jones, Spherical bioactive glass particles and their interaction with human mesenchymal stem cells in vitro, Biomaterials 32 (2011) 1010–1018.

[27] B. Marelli, C.E. Ghezzi, D. Mohn, W.J. Stark, J.E. Barralet, A.R. Boccaccini, Showan N. Nazhat, Accelerated mineralization of dense collagen-nano bioactive glass hybrid gels increases scaffold stiffness and regulates osteoblastic function, Biomaterials 32 (2011) 8915–8926.

[28] M. Sohrabi, S. Hesaraki, A. Kazemzadeh, M. Alizadeh, Development of injectable biocomposites from hyaluronic acid and bioactive glass nano-particles obtained from different sol-gel routes, Mater. Sci. Eng., C Mater. Biol. Appl. 33 (2013) 3730–3744.

[29] A. El-Fiqi, T.H. Kim, M. Kim, M. Eltohamy, J.-E. Won, E.J. Lee, H.W. Kim, Capacity of mesoporous bioactive glass nanoparticles to deliver therapeutic molecules, Nanoscale 4 (2012) 7475–7488.

[30] E. Mir, A. Hossein-Nezhad, A. Bahrami, M.R. Bekheirnia, E. Javadi, A.A. Naderi, Adequate serum copper concentration could improve bone density, postpone bone loss and protect osteoporosis in women, Iran. J. Public Health (2007) 24–29.

[31] T. Wilson, J.M. Katz, D.H. Gray, Inhibition of active bone-resorption by copper, Calcif. Tissue Int. 33 (1981) 35–39.

[32] M. Shi, Z. Chen, S. Farnaghi, T. Friis, X. Mao, Y. Xiao, C. Wu, Copper-doped mesoporous silica nanospheres, a promising immunomodulatory agent for inducing osteogenesis, Acta Biomater. 30 (2016) 334–344.

[33] T. Kokubo, H. Takadama, How useful is SBF in predicting in vivo bone bioactivity?, Biomaterials 27 (2006) 2907–2915

[34] A.L.B. Maçon, T.B. Kim, E.M. Valliant, K. Goetschius, R.K. Brow, D.E. Day, A. Hoppe, A.R. Boccaccini, I.Y. Kim, C. Ohtsuki, T. Kokubo, A. Osaka, M. Vallet-Regí, D. Arcos, L. Fraile, A.J. Salinas, A.V. Teixeira, Y. Vueva, R.M. Almeida, M. Miola, C. Vitale-Brovarone, E. Verné, W. Höland, J.R. Jones, A unified in vitro evaluation for apatite-forming ability of bioactive glasses and their variants, J. Mater. Sci.: Mater Med 26 (2015) 115.

[35] M.S. Sbarra, C.R. Arciola, A. Di Poto, E. Saino, H. Rohde, P. Speziale, L. Visai, The photodynamic effect of tetra-substituted N-methyl-pyridyl-porphine combined with the action of vancomycin or host defense mechanisms disrupts Staphylococcus epidermidis biofilms, Int. J. Artif. Organs 32 (2009) 574–583.

[36] P. Chaignon, I. Sadovskaya, C. Ragunah, N. Ramasubbu, J.B. Kaplan, S. Jabbouri, Susceptibility of staphylococcal biofilms to enzymatic treatments depends on their chemical composition, Appl. Microbiol. Biotechnol. 75 (2007) 125–132.

[37] H. Malekinejad, B. Bazargani-Gilani, A. Tukmechi, H. Ebrahimi, A cytotoxicity and comparative antibacterial study on the effect of Zataria multiflora Boiss, Trachyspermum copticum essential oils, and Enrofloxacin on Aeromonas hydrophila, Avicenna J. Phytomed. 2 (2012) 188–195.

[38] E. Saino, M.S. Sbarra, C.R. Arciola, M. Scavone, N. Bloise, P. Nikolov, F. Ricchelli, L. Visai, Photodynamic action of Tri-meso (N-methyl-pyridyl), meso (N-tetradecyl-pyridyl) porphine on Staphylococcus epidermidis biofilms grown on Ti6Al4V alloy, Int. J. Artif. Organs 33 (9) (2010) 636–645.

[39] H.J. Busscher, H.C. van der Mei, Microbial adhesion in flow displacement systems, Clin. Microbiol. Rev. 19 (2006) 127–141.

[40] A. Cochis, B. Azzimonti, R. Sorrentino, C. Della Valle, E. De Giglio, N. Bloise, L. Visai, G. Bruni, S. Cometa, D. Pezzoli, G. Candiani, L. Rimondini, R. Chiesa, Data in support of Gallium (Ga(3+)) antibacterial activities to counteract E. coli and S. epidermidis biofilm formation onto pro-osteointegrative titanium surfaces, Data Brief 6 (2016) 758–762.

[41] A.J. Salinas, S. Shruti, G. Malavasi, L. Menabue, M. Vallet-Regí, Substitutions of cerium, gallium and zinc in ordered mesoporous bioactive glasses, Acta Biomater. 7 (2011) 3452–3458.

[42] F.E. López-Suárez, S. Parres-Esclapez, A. Bueno- López, M.J. Illán-Gómez, B. Ura, J. Trawczynski, Role of surface and lattice copper species in copper-containing (Mg/Sr) TiO3 perovskite catalysts for soot combustion, Appl. Catal. B: Environ. 93 (2009) 82–89.

[43] B.E. Goodby, J.E. Pemberton, XPS characterization of a commercial Cu/ZnO/Al2O3 catalyst: effects of oxidation, reduction and the steam reformation of methanol, Appl. Spectrosc. 42 (1988) 754–760.

[44] H. Zhang, C. Tang, Y. Lv, C. Sun, F. Gao, L. Dong, Y. Chen, Synthesis, characterization, and catalytic performance of copper-containing SBA-15 in the phenol hydroxylation, J. Colloid Interface Sci. 380 (2012) 16–24.

[45] A. Martínez, I. Izquierdo-Barba, M. Vallet-Regí, Bioactivity of a CaO-SiO2 binary glasses system, Chem. Mater. 12 (2000) 3080–3088.

[46] P. Siriphannon, Y. Kameshima, A. Yasumori, K. Okada, S. Hayashi, Formation of hydroxyapatite on CaSiO3 powders in simulated body fluid, J. Eur. Ceram. Soc. 22 (2002) 511–520.

[47] M. Mozafari, F. Moztarzadeh, M. Tahriri, Investigation of the physico-chemical reactivity of a mesoporous bioactive SiO2–CaO–P2O5 glass in simulated body fluid, J. Non-Cryst. Solids 356 (2010) 1470–1478.

[48] H. Ohgushi, M. Okumura, T. Yoshikawa, K. Inoue, N. Senpuku, S. Tamai, E.C. Shors, Bone formation process in porous calcium carbonate and hydroxyapatite, J. Biomed. Mater. Res. 26 (1992) 885–895.

[49] Y. Fujita, T. Yamamuro, T. Nakamura, S. Kotani, C. Ohtsuki, T. Kokubo, The bonding behavior of calcite to bone, J. Biomed. Mater. Res. 25 (1991) 991–1003.

[50] M. Mami, A. Lucas-Girot, H. Oudadesse, R. Dorbez-Sridi, F. Mezahi, E. Dietrich, Investigation of the surface reactivity of a sol-gel derived glass in the ternary system SiO2–CaO–P2O5, Appl. Surf. Sci. 254 (2008) 7386–7393.

[51] E.A. Neel, I. Ahmed, J. Pratten, S.N. Nazhat, J.C. Knowles, Characterisation of antibacterial copper releasing degradable phosphate glass fibres, Biomaterials 26 (2005) 2247–2254.

[52] S. Jaiswal, P. McHale, B. Duffy, Preparation and rapid analysis of antibacterial silver, copper and zinc doped sol-gel surfaces, Colloids Surf. B. Biointerfaces 94 (2012) 170–176.

[53] C.Y. Chen, C.L. Chiang, Preparation of cotton fibers with antibacterial silver nanoparticles, Mater. Lett. 62 (2008) 3607–3609.

[54] H. Palza, S. Gutierrez, K. Delgado, O. Salazar, V. Fuenzalida, J. Avila, G. Figueroa, R. Quijada, Toward tailor-made biocide materials based on polypropylene/copper nanoparticles, Macromol. Rapid Commun. 31 (2010) 563–569.

[55] S. Shrivastava, T. Bera, A. Roy, G. Singh, P. Ramachandrarao, D. Dash, Characterization of enhanced antibacterial effects of novel silver nanoparticles, Nanotechnology 18 (2007) 225103.

[56] H. Li, Q. Chen, J. Zhao, K. Urmila, Enhancing the antimicrobial activity of natural extraction using the synthetic ultrasmall metal nanoparticles, Sci. Rep. (2015) 11033.

[57] Y.E. Lin, R.D. Vidic, J.E. Stout, C.A. Mccartney, V.L. Yu, Inactivation of Mycobacterium avium by copper and silver ions, Water Res. 32 (1998) 1997–2000.

[58] E. Ladomersky, M.J. Petris, Copper tolerance and virulence in bacteria, Metallomics 7 (2015) 957–964.

[59] S. Hu, J. Chang, M. Liu, C. Ning, Study on antibacterial effect of 45S5 Bioglass, J. Mater. Sci. Mater Med. 20 (2009) 281–286.

[60] V. Mortazavi, M.M. Nahrkhalaji, M.H. Fathi, S.B. Mousavi, B.N. Esfahani, Antibacterial effects of sol-gel-derived bioactive glass nanoparticle on aerobic bacteria, J. Biomed. Mater. Res. 94 (2010) 160–168.

[61] M. Raffi, S. Mehrwan, T.M. Bhatti, J.I. Akhter, A. Hameed, W. Yawar, M. Masood ul Hasan, M. , Investigations into the antibacterial behavior of copper nanoparticles against Escherichia coli, Ann. Microbiol. 60 (2010) 75–80.

[62] J.W. Costerton, P.S. Stewart, E.P. Greenberg, Bacterial biofilms: a common cause of persistent infections, Science 284 (1999) 1318–1322.

[63] I. Armentano, C.R. Arciola, E. Fortunati, D. Ferrari, S. Mattioli, C.F. Amoroso, J. Rizzo, J.M. Kenny, M. Imbriani, L. Visai, The interaction of bacteria with engineered nanostructured polymeric materials: a review, Sci. World J. 2014 (2014) 410–423.

[64] I. Keren, N. Kaldalu, A. Spoering, Y. Wang, K. Lewis, Persister cells and tolerance to antimicrobials, FEMS Microbiol. Lett. 230 (2004) 13–18.

[65] C.A. Fux, J.W. Costerton, P.S. Stewart, P. Stoodley, Survival strategies of infectious biofilms, Trends Microbiol. 13 (2005) 34–40.

[66] Y.M. Mohan, K. Lee, T. Premkumar, K.E. Geckeler, Hydrogel networks as nonreactors: a novel approach to silver nanoparticles for antibacterial applications, Polymer 48 (2007) 158–164.

[67] S.M. Dizaj, F. Lotfipour, M. Barzegar-Jalali, M.H. Zarrintan, K. Adibkia, Antimicrobial activity of the metals and metal oxide nanoparticles, Mater. Sci. Eng. C. Mater. Biol. Appl. 44 (2014). 278-184.

[68] E. Fortunati, S. Rinaldi, M. Peltzer, N. Bloise, L. Visai, I. Armentano, A. Jimenez, L. Latterini, J. Kenny, Nano-biocomposite films with modified cellulose nanocrystals and synthesized silver nanoparticles, Carbohydr. Polym. 101 (2014) 1122–1133.

[69] D. Longano, N. Ditaranto, L. Sabbatini, L. Torsi, N. Cioffi, Synthesis and antimicrobial activity of copper nanomaterials, Nano-Antimicrob.: Progr. Prospect. 3 (2012) 85–117.

[70] M.E. Villanueva, A.M. Diez, J.A. Gonzàlez, C.J. Pérez, M. Orrego, L. Piehl, S. Teves, G.J. Copello, Antimicrobial activity of starch hydrogel incorporated with copper nanoparticles, ACS Appl. Mater. Interfaces 8 (2016) 16280–16288.